Electrochimica Acta 185 (2015) 117–124

Contents lists available at ScienceDirect

Electrochimica Acta

journal homepage: www.elsevier.com/locate/electacta

A New Si/TiO_2/Pt p-n Junction Semiconductor to Demonstrate Photoelectrochemical CO_2 Conversion

Thaís Tasso Guaraldo[a,b,1], Juliana Ferreira de Brito[a,1,*], David Wood[b], Maria Valnice Boldrin Zanoni[a]

[a] UNESP, Chemistry Institute of Araraquara, R. Francisco Degni 55, 14800-060 Araraquara, SP, Brazil
[b] School of Engineering and Computing Sciences, Durham University, South Road, Durham, England DH1 3LE, United Kingdom

ARTICLE INFO

Article history:
Received 26 May 2015
Received in revised form 29 August 2015
Accepted 16 October 2015
Available online 4 November 2015

Keywords:
Si/TiO_2/Pt
heterojunction
CO_2 reduction
photoelectrocatalysis

ABSTRACT

This work presents a new Si/TiO_2/Pt p-n junction semiconductor prepared by sputtering, chemical vapor deposition (CVD), photolithography and lift-off techniques. XRD, EDS, FE-SEM, diffuse reflectance (DRS) and photocurrent vs potential curves had been used for semiconductor characterization. The material was designed for high porosity and uniformity of both TiO_2 and Pt deposits; both TiO_2 anatase phase formation and Pt presence were confirmed. This semiconductor has a characteristic of high light absorption in the ultraviolet and visible regions. A good photocurrent response for the cathodic region was obtained in a CO_2 saturated solution (−1.0 mA under −0.8 V and UV–vis light), confirming electron-hole pair formation and CO_2 electron scavenging. A small Si/TiO_2/Pt electrode (1 × 1 cm) was employed in photoelectrocatalytic CO_2 reduction, forming methanol (0.88 mmol L^{-1}), ethanol (2.60 mmol L^{-1}) and acetone (0.049 mmol L^{-1}) as products reaching a Faradaic efficiency of 96.5%. These results had been obtained under the following optimal experimental conditions: 0.1 mol L^{-1} $NaHCO_3$, pH 8 saturated with CO_2, 125 W UV–vis irradiation (from 250 to 600 nm) and −0.8 V applied potential. Suitable charge transfer mechanisms in the electrode surface, and products formation after CO_2 reduction, are proposed.

1. Introduction

The increase of global warming is one of the major concerns of the modern world [1–3] and consequently the conversion of CO_2 into value added products and/or high-energy content fuel is one of the goals in environmental research [4]. Because of this reason, since 1978, when the first research was published concerning CO_2 conversion using photoelectrocatalytic reduction [5], many different p-type semiconductors have been studied for this application.

Among the various possible approaches, photoelectrocatalysis [6,5,7,8] have been demonstrated as promising technique, mainly because this method has advantages over CO_2 reduction that can be tuned by using different materials as a photocatalyst when combined with light irradiation and potential application. This simple arrangement is able to provide electrons and reactive intermediates able to produce several kinds of hydrocarbons, for instance [9,10].

Halmann [5] in the pioneering paper about photoelectrocatalytic CO_2 reduction, presented the study of GaP as p-type semiconductor for this purpose. Inoue and coworkers [8] presented one year later the application of the same semiconductor for photoelectrocatalytic CO_2 conversion, although other semiconductors as WO_3, TiO_2, ZnO, CdS, GaP and SiC were also applied in CO_2 conversion using photocatalysis.

Currently, p-type semiconductors based on copper and copper oxides [9–17] are the most widely known p-type electrode used for CO_2 reduction. Although these semiconductors had shown good performance on CO_2 reduction, in recent years the search for more stable semiconductors for photoelectrochemical reduction is still an issue in this field [18–20]. From this, some groups have presented the combination of metals and oxides seeking robust materials. Cheng et al. [21] employed Pt-modified reduced graphene oxide for photoelectrocatalytic CO_2 reduction. Yang et al. [22] performed photoelectrocatalytic CO_2 reduction using one-dimensional ribbon CoPc enhanced Fe_2O_3 nanotubes, and Li and coworkers [2] prepared TiO_2 nanotubes modified with a CdSeTe nanosheet aiming at photoelectrocatalytic CO_2 reduction.

Another strategy highlighted recently is the application of heterojunctions for the achievement of electrodes with more stability. In this kind of semiconductor the electron present in the

* Corresponding author. Tel.: +55 16 33019740.
E-mail address: jfbrito@ymail.com (J.F.d. Brito).
[1] First coauthor: both first and second authors contributed equally to this work.

http://dx.doi.org/10.1016/j.electacta.2015.10.077
0013-4686/

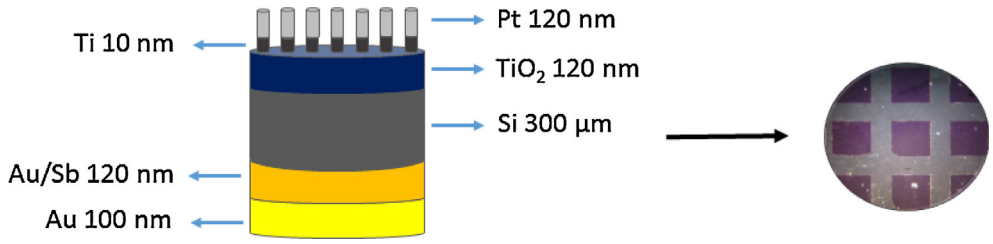

Fig. 1. A graphical view scheme of the Si/TiO_2/Pt structure and an approximated real view of the surface semiconductor.

conduction band of the n-type semiconductor is directed to the valence band of the p-type semiconductor, thus the electrons and the holes photogenerated are spatially separated minimizing the recombination [1,23]. Moreover, the heterojunctions provide enhanced irradiation absorption and charges transfer efficiency for the semiconductors, as well as photocorrosion stability and consequently photocatalytic efficiency [24,25].

In this sense, the semiconductor silicon has the interesting properties of mechanical strength, high thermal conductivity, a wide electrical conductivity range and, for the purposes of this work, versatile optical characteristics [26]. However, this material has poor chemical stability and can be easily oxidized in aqueous solution under applied potential [24,23,27,28]. Nevertheless, the stability and unusual electrocatalytic properties can be obtained with a composite anode based on a TiO_2 and Si heterojunction [28,29]. A union of these features demonstrated great potential for photoelectrochemical purposes. In agreement with the literature [23] for a n-Si/n-TiO_2 heterojunction, the photogenerated holes under positive potential move toward the n-TiO_2/electrolyte interface where an oxidation reaction takes place. Therefore, the photogenerated electrons in the n-Si move to the counter electrode, where the reduction reaction takes place. For p-Si/n-TiO_2 junctions, the flow of electrons and holes at the junction occurs in the opposite direction, generating a smaller photoanodic current density.

Christensen et al. [28] has demonstrated that a composite anode based on TiO_2 and Si heterojunction coupled to metal grid (n-Si/TiO_2/Au) has great potential as a photoanode, where holes generated in the n-Si layer can be accelerated to the surface of the TiO_2 by an applied potential. The metal grid combination with an applied potential facilitated the transport of holes from the Si to the TiO_2 surface, and the spill over from the TiO_2 to the metal grid, culminating in the generation of active chemical species at the semiconductor surface [28]. While the heterojunction of p-Si/TiO_2 semiconductor has different band bending properties near the junction [23], which enhances the charge separation and minimize recombination within the material. This behavior enhances the possibility of increasing electrons flow at the material semiconductor surface. Consequently, it could be a good option to promote photoreduction addressed to CO_2 conversion for instance.

TiO_2 band gap engineering has been reported in the literature for CO_2 photocatalytic conversion. TiO_2/SiO_2 and Ru doped, Pt-TiO_2/glass bead and Pt/TiO_2 nanotubes supported photocatalysts are reported by Liu and collaborators for CO_2 conversion [30]. However, Si/TiO_2/Pt photocathode for photoelectrochemical carbon dioxide conversion has not been referenced. Additionally, a small number of materials are described for photoelectrocatalytic CO_2 reduction.

The present work investigates the development of a novel composite cathode Si/TiO_2/Pt p-n junction semiconductor prepared by sputtering, CVD and photolithography techniques and its application on the photoelectrocatalytic CO_2 conversion, aiming to generated products with high added value, such as ethanol.

2. Experimental

2.1. Preparation of the new p-n junction Si/TiO_2/Pt electrode

The composite p-Si/TiO_2/Pt electrodes was obtained by using an adapted methodology described in literature [28]. Firstly, the p-type Si wafer substrate (2.0 inches) was carefully cleaned in a H_2O_2:H_2SO_4 (1:1) solution during 30 min, washed with deionized water and treated during 2 min in HF:H_2O (1:10) solution with the aim of removing the native SiO_2 layer from the wafer surface. Afterwards the wafer was rinsed in deionized water, and a TiO_2 layer (120 nm) was deposited by sputtering (Moorfield Minilab 3 sputtering system). Argon was used as the sputtering gas, the target was TiO_2 and the pressure was maintained at 2 mT during deposition at room temperature. The wafer was then annealed at 450 °C for 30 min under N_2 flow. The back contact was composed of a Au/Sb layer (200 nm) alloyed at 400 °C for 15 min and a further Au

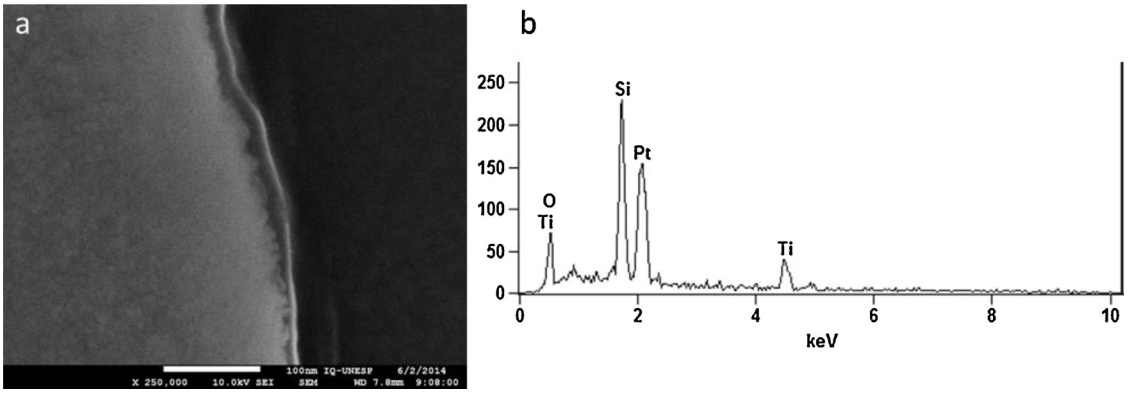

Fig. 2. (a) FE-SEM image and (b) EDS analysis presenting the interface TiO_2-Pt of the Si/TiO_2/Pt semiconductor.

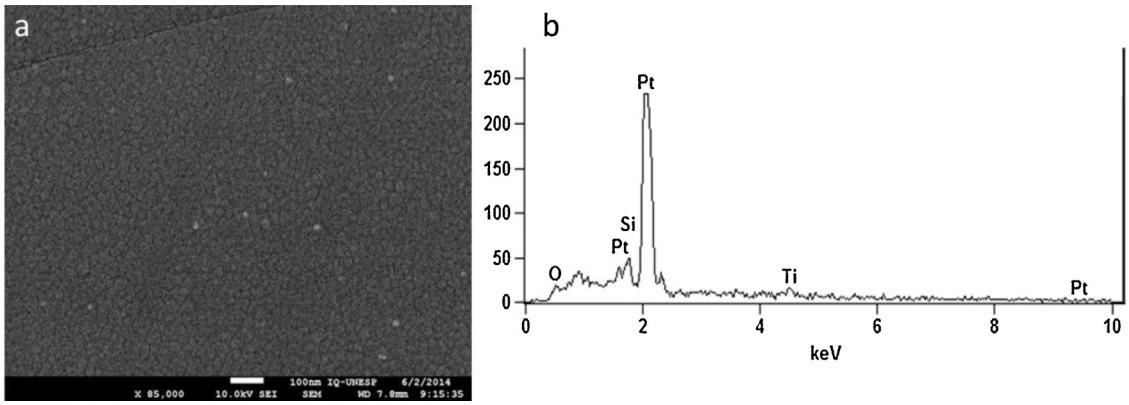

Fig. 3. (a) FE-SEM image and (b) EDS analysis of the Si/TiO_2/Pt semiconductor showing the Pt deposit region.

layer (100 nm), both deposited by e-beam evaporation. Two different photoresists (SF9 and SPR350) were spin coated on the TiO_2 surface and baked. The wafer was then placed in a mask aligner for to expose the pattern for the grid electrode. The pattern was developed in a solution of MF319 developer, and the wafer given a further bake. A Ti seed layer (10 nm) was e-beam deposited for better grid adhesion, followed by a 120 nm Pt grid layer. The grid was produced by lifting off the photoresist in NMP, followed by final rinsing in acetone, isopropanol and deionized water. A graphical view and an approximated real view of the surface semiconductor are presented in the Fig. 1.

2.2. Characterization of the new p-n junction Si/TiO_2/Pt electrode

The new p-n junction Si/TiO_2/Pt was characterized by X-ray diffraction recorded on a Siemens Model D 5000 diffractometer. The structures and morphologies were analyzed by field emission scanning electron microscopy (FE-SEM) on a Zeiss model Supra 35 equipped with an energy dispersive X-ray (EDX) spectrometer. Diffuse reflectance spectroscopy was performed in both the infrared and visible regions. Linear sweep voltammetry was carried out at 0.01 V s^{-1} scan rate, in the absence and presence of UV–vis radiation in 0.1 mol L^{-1} sodium bicarbonate solution as supporting electrolyte, with the supporting electrolyte saturated with CO_2.

2.3. Apparatus and procedure for photoelectrochemical CO_2 reduction

The photoelectrocatalytic CO_2 reduction experiments were performed in a cylindrical two-compartment glass reactor equipped with a cooling system. The sample of p-Si/TiO_2/Pt (1 × 1 cm) was inserted in one compartment of the photoelectrocatalytic reactor (400 mL) as a working electrode with a saturated Ag/AgCl (KCl sat) electrode as the reference. The working electrode was irradiated by a commercial 125 W UV–vis light with irradiance of 21 mW cm^{-2} without the bulb vertically inserted in a central quartz bulb. A Pt gauze counter electrode (2 × 2 cm) was inserted in the other photoelectrocatalytic compartment. Controlled-potential electrolysis was carried out using a potentiostat Autolab model PGSTAT 302 under a controlled potential of −0.8 V. The photoelectrocatalytic treatment was carried out for dissolved CO_2 gas (OXI-MEDIN) at room temperature in 0.1 mol L^{-1} $NaHCO_3$ as the supporting electrolyte. Aliquots of the solution were taken at controlled times and products evaluated.

2.4. Product profiles in photoelectrochemical CO_2 reduction

Methanol (CH_3OH), ethanol (C_2H_5OH) and acetone (CH_3COCH_3) were analyzed by gas chromatography on a Model CG-2010 Schimadzu instrument coupled with a flame ionization detector employing the solid-phase micro-extraction technique (SPME) [9]. For this purpose, a 0.5 mL aliquot of the photoelectrolyzed solution was transferred to a sealed container (1.5 mL) and submitted to a heated bath for 7 min at 65 °C. After this time, the fiber (75 μm Carboxen/PDMS, SUPELCO) was exposed to the container vapors for 5 min and the vapors injected into the gas chromatograph. The chromatographic column employed was Stabilvax RESTEC 30 m length, 0.25 mm internal diameter and 25 mm film thickness. Nitrogen was used as carrier gas at 1.0 mL min^{-1} flow rate. The injector was maintained at 250 °C and the detector at 260 °C in the splitless mode. The heating ramp used is as follows: 35 °C for 4 min, 45 °C at 2 °C min^{-1}, 120 °C at 30 °C min^{-1} and 120 °C for 3 min. Analytical curves were constructed and linear relationship was

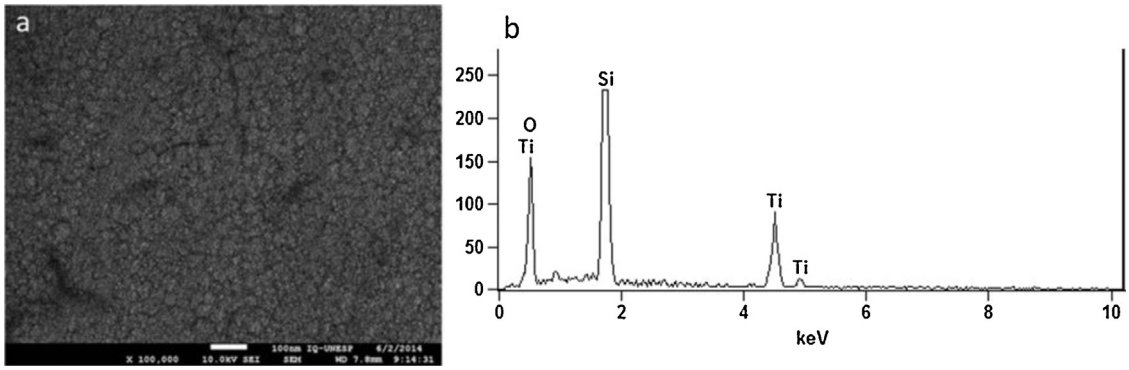

Fig. 4. (a) FE-SEM image and (b) EDS analysis of the Si/TiO_2/Pt semiconductor showing the TiO_2 deposit region.

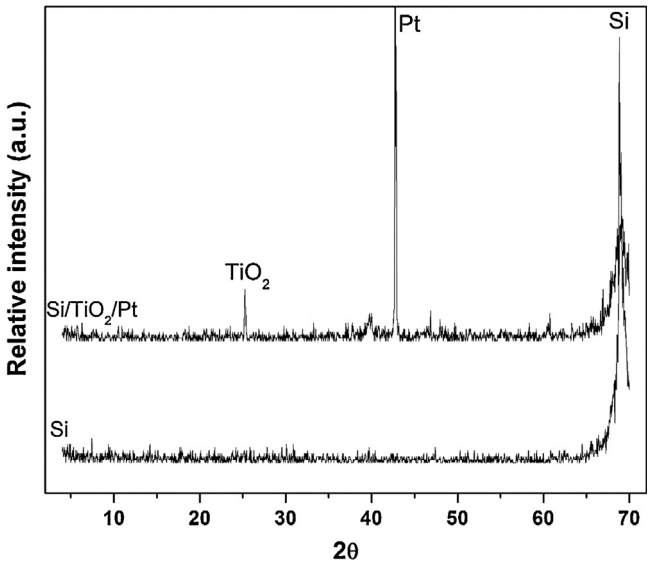

Fig. 5. XRD diffractogram of the $Si/TiO_2/Pt$ semiconductor and the Si substrate.

obtained for acetone in the range of 0.5 μmol L^{-1} to 0.1 mmol L^{-1}, with 0.01 to 10.0 mmol L^{-1} for methanol and 0.05 to 7.5 mmol L^{-1} for ethanol. The determination coefficients and quantification limits were 0.9854 and 0.05 μmol L^{-1} for acetone, 0.9971 and 0.1 mmol L^{-1} for methanol, 0.9856 and 0.05 mmol L^{-1} for ethanol, respectively.

3. Results and discussions

3.1. p-n $Si/TiO_2/Pt$ semiconductor features

Fig. 2a illustrates the top view FE-SEM image obtained for the TiO_2/Pt interface of the p-n $Si/TiO_2/Pt$ semiconductor prepared in this study. The presence of Pt and TiO_2 in the semiconductor interface was confirmed by the EDS analysis (Fig. 2b). The preparation route led to two different areas, as can be observed in Fig. 2a. The left side of the image corresponds to the Pt nanoparticulated area, proven by the EDS results presented in Fig. 3b. A FE-SEM image of the main Pt area is shown in Fig. 3a. The right area of the Fig. 2a image is relative to TiO_2 nanoparticles deposition, which can be confirmed by FE-SEM micrographs and EDS analysis in Fig. 4.

Material crystallinity was confirmed by XRD (Fig. 5). The diffractogram of the p-n junction $Si/TiO_2/Pt$ semiconductor shows three defined peaks. The peak $2\theta = 25°$ is relative to the TiO_2 anatase phase, the most photoactive phase of this oxide [31]. The peak $2\theta = 43°$ is attributed to Pt, and $2\theta = 70°$ relative to Si. The substrate line in Fig. 4 show the peak for Si without modification ($2\theta = 70°$) which was suppressed after the TiO_2 and Pt depositions.

3.2. Si/TiO2/Pt behavior under UV–vis irradiation and effect of CO_2 in the photocurrent/voltage curves

Diffuse reflectance analysis was conducted for a standard Si substrate and for the p-n junction $Si/TiO_2/Pt$, for evaluation of the semiconductor behavior upon UV–vis irradiation (Fig. 6a). The Si substrate presents high values of optical absorption (dashed curve) in all spectra (200 to 800 nm) mainly in the ultraviolet region. However, deposition of TiO_2 and Pt on the substrate causes an increase in optical absorption in the visible region, with two bands around 400 nm and 500 nm, maintaining higher optical absorption in the ultraviolet regions ($\leq$ 380 nm) and showing material absorbs in the visible light region. Material absorption from 650 nm has also improved. This behavior indicates the material shows excellent optical properties and could absorb light over a wide spectrum. As the lamp source used in this work emits in this region (UV and vis), there is suitable use of light for photoelectrochemical purposes. This behavior is in agreement with high faradaic efficiency obtained in this study possibly due to high photonic efficiency conversion of p-n junction. Electrons are accumulated at Pt surface increasing CO_2 reduction kinects at Pt/electrolyte interface.

The inset in Fig. 6(a) shows the Tauc's graph [32] used to estimate the bandgap energy of the material. The diffuse reflectance measurements were converted to an equivalent absorption coefficient by the Kubelka-Munk equation:

$$\alpha = (1 - R)^{1/\gamma}/2R \quad (1)$$

Where α is the material absorptivity, R is the reflectance and γ is the power coefficient, which can assume the values 1/2, 3/2, 2 or 3 according to the electronic transition type: direct allowed, direct forbidden, indirect allowed and indirect forbidden, respectively

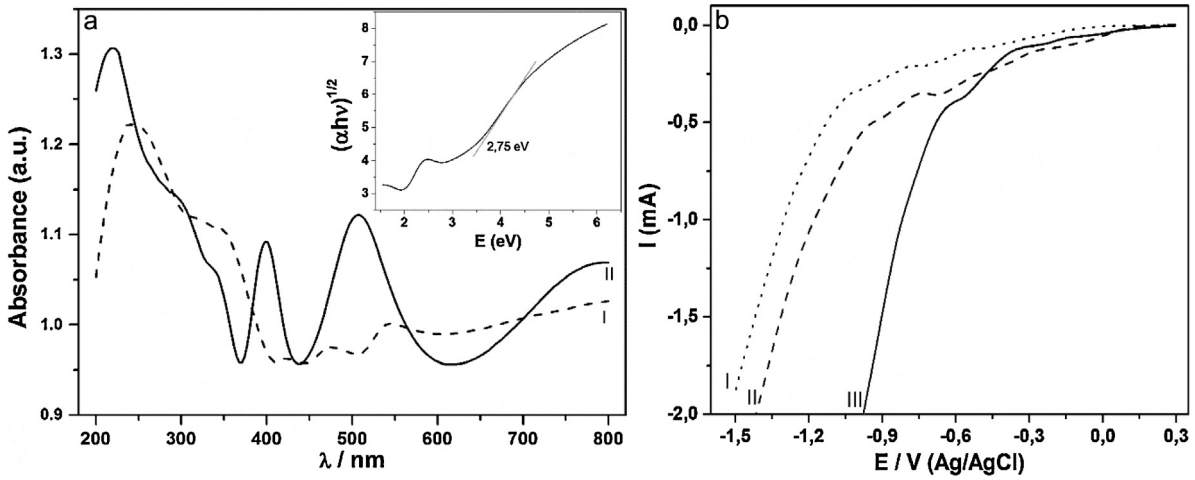

Fig. 6. The p-n junction $Si/TiO_2/Pt$ (a) diffuse reflectance analysis of p-Si (line I) and p-n $Si/TiO_2/Pt$ (II) with an insert of the material band gap and (b) photocurrent vs. potential under dark (line I), under UV–vis light (line II) and under UV–vis light with supporting electrolyte saturated with CO_2 (line III).

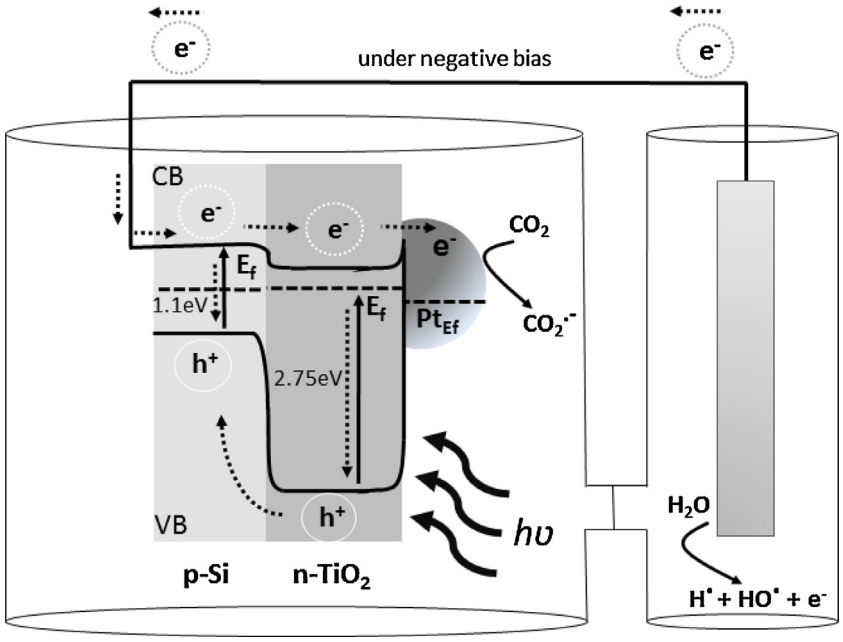

Fig. 7. Charge transfer mechanism for the p-n junction $Si/TiO_2/Pt$ semiconductor.

[33,34]. More accurate results in the case of a TiO_2 semiconductor are obtained considering the indirect allowed transition ($\gamma = 2$) [35]. The p-n junction $Si/TiO_2/Pt$ revealed a band gap value of 2.75 eV as presented in the inset of Fig. 5a. The commonly reported band gap value for TiO_2 anatase is 3.2 eV [36–38]. The difference between the TiO_2 anatase and $Si/TiO_2/Pt$ band gap values can be attributed to doping of the TiO_2 with Pt, which introduces an intragap energy level inside the TiO_2 band gap [39]. This behavior contributes to the absorption threshold of ultraviolet towards visible, in addition to a reduction of the material band gap [39].

Fig. 6b shows typical photocurrent *vs*. potential curves obtained for a $Si/TiO_2/Pt$ semiconductor in 0.1 mol L^{-1} $NaHCO_3$ solution in dark conditions (I) and irradiated by UV–vis light before (II) and after (III) saturation with CO_2. A shift towards a less negative potential is observed when the semiconductor is activated by light, indicating that electrons and holes pairs (e^-/h^+) are created inside both Si and TiO_2 due to irradiation in UV–vis region. The TiO_2 is activated by the UV light and visible light can be harvested by the Si [23]. The photogenerated electrons moves toward the Pt/electrolyte interface [28], where water reduction can takes place to generate hydrogen [22,40].

Fig. 7 illustrates the process. In the presence of CO_2 the curve leads to a larger negative onset potential (from −1 to −0.5 V vs Ag/AgCl), indicating the p-n junction promotes more effective separation of photogenerated charges. This indicates that the flat band potential of the semiconductor is lower than the hydrogen reduction potential and CO_2 could be attracted to the $Si/TiO_2/Pt$ surface, but requires an external applied potential higher than −0.4 V (Curve III, Fig. 5b). This fact indicates that CO_2 acts as much better electron scavenger (capturing the photoelectrons generated by e^-/h^+ separation from $Si/TiO_2/Pt$) than water [2,40]. $Si/TiO_2/Pt$ under CO_2, light and −0.8 V potential conditions produces a

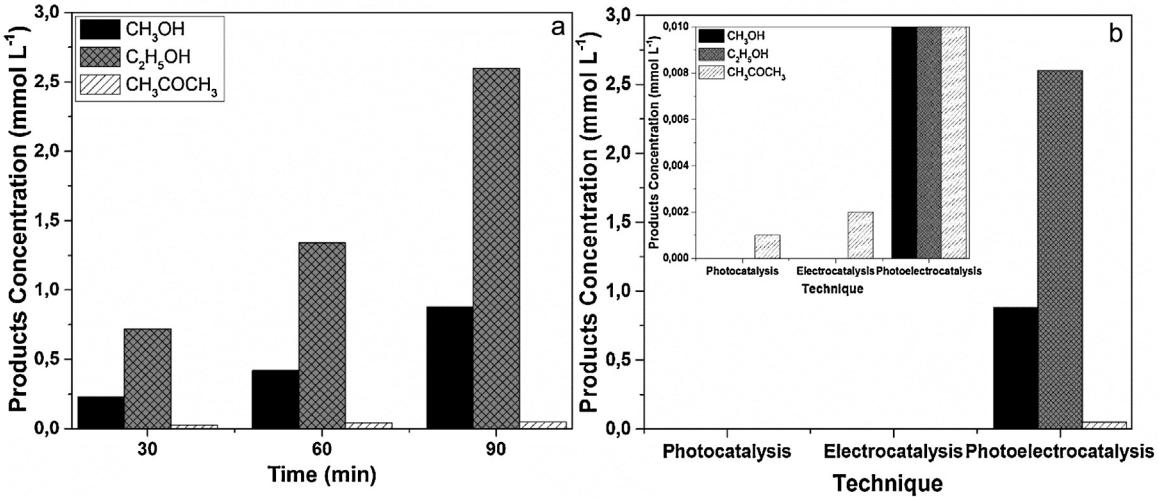

Fig. 8. a) CO_2 conversion into the products methanol (CH_3OH), ethanol (C_2H_5OH) and acetone (CH_3COCH_3) in different times and applying photoelectrocatalysis at −0.8 V and 0.1 mol L^{-1} $NaHCO_3$, pH 8, and b) comparison between the photocatalysis, electrocatalysis and photoelectrocatalysis technique under the same conditions.

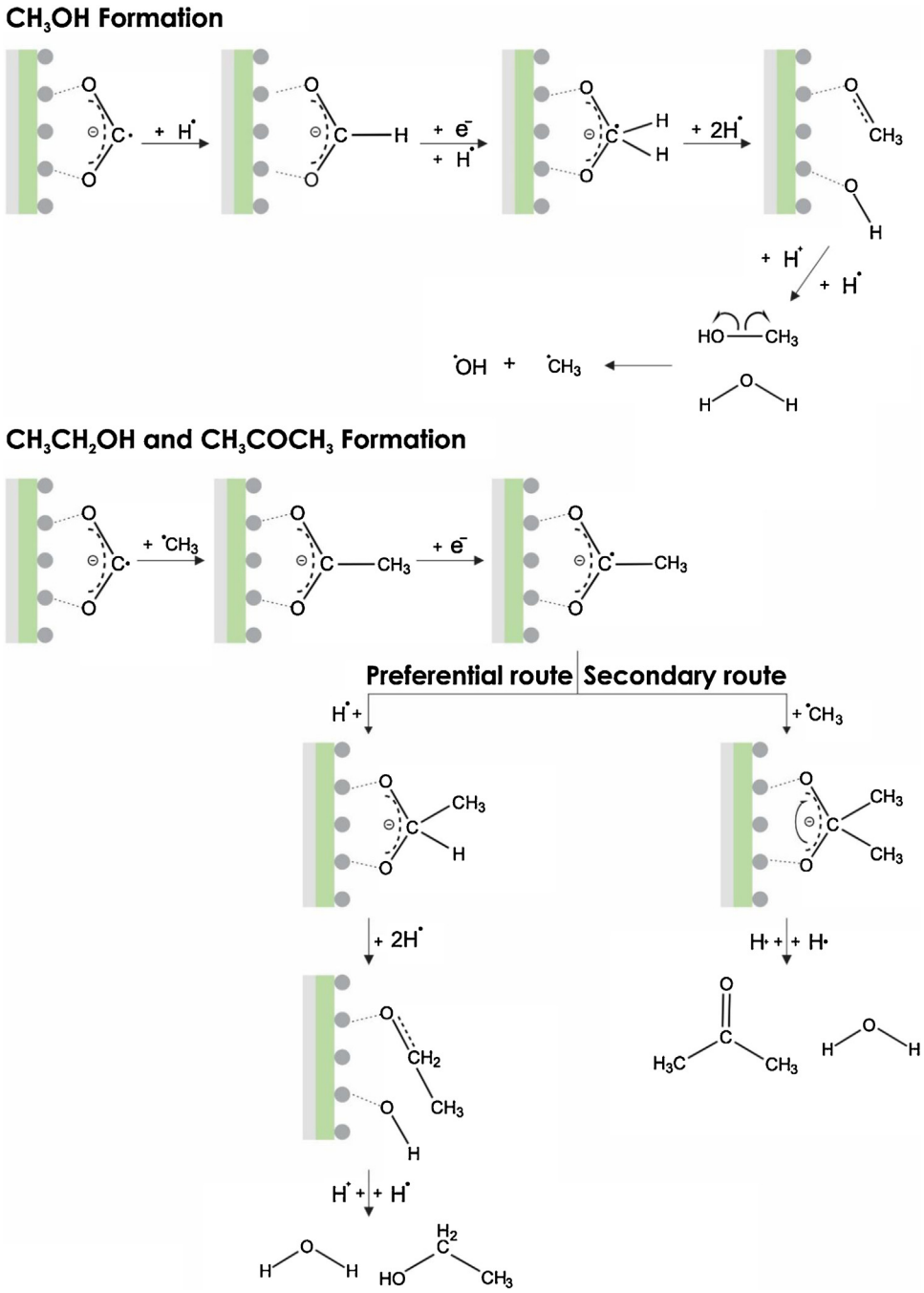

Fig. 9. Mechanism proposed for methanol, ethanol and acetone formation from the photoelectrocatalytic CO_2 reduction applied to the p-n junction $Si/TiO_2/Pt$ semiconductor.

current 5 times higher than the semiconductor without CO_2 and light application, and 3 times more intense than under light without CO_2 saturation. Based on this results, this condition (−0.8 V) was chosen for photoelectrocatalytic CO_2 reduction experiments, a potential considerably smaller than the thermodynamic potential (vs NHE) necessary for the CO_2 reduction [41].

The photoactivity results suggested that a p-n heterojunction $Si/TiO_2/Pt$ electrode acts as very efficient cathode under negative applied potential. The charge transfer mechanism proposed for $Si/TiO_2/Pt$ p-n heterojunction presented in Fig. 7 was proposed based in the research of Hwang and coworkers [23], where the electrons generated by a negative applied potential and light incidence in both surfaces, Si and TiO_2, move to lower energy levels and are consequently trapped by the Pt due to a lower Fermi level. The opposite behavior occurs for holes formed at the semiconductor surface. Therefore, electrons move from the counter electrode towards the working electrode while holes are generated at the photocathode and reach the Pt counter electrode in order to undertake oxidation reactions. Under negative applied, electron/hole pair recombination is minimized by more efficient charge separation, favoring photoelectrocatalysis target [33,42]. The CO_2 reduction occurs at the Pt surface, where it is converted to $^{\bullet}CO_2^-$ [43,40,44,45] and hence protonation and deprotonation reactions occur to form the products [10,46]. The overall charge transfer mechanism characterizes the p-n junction [47].

3.3. Photoelectrochemical CO_2 conversion

The photoelectrocatalytic CO_2 conversion in methanol, ethanol and acetone was monitored during 90 min of photoelectrolysis on a $Si/TiO_2/Pt$ electrode in 0.1 mol L^{-1} $NaHCO_3$ pH 8 saturated with CO_2 (Fig. 8a) under an applied potential of −0.80 V and UV–vis irradiation. These conditions were chosen based in our previously knowledge in the photoelectrocatalytic CO_2 reduction [9,10]. The $NaHCO_3$ is a better supporting electrolyte for CO_2 solubilization, due to the chemical equilibrium, allowing a greater CO_2 amount in solution [48]. The equilibrium of species present in the medium is affected by the supporting electrolyte pH owing to the dynamic equilibrium for CO_2 dissolved. At pH 8, the following equilibrium is obtained: $CO_2 + H_2O \leftrightarrow H_2CO_3 \leftrightarrow H^+ + HCO_3^-$ [49], these species are responsible by scavenging $OH^\bullet$ and prevent further oxidation of the products formed in addition to favoring alcohols formation [10].

The first 30 min of reaction led to the formation of 0.23 mmol L^{-1} of methanol, 0.72 mmol L^{-1} of ethanol and 0.025 mmol L^{-1} of acetone. After 60 min, all the products formation increased, reaching maximum values at 90 min of reaction with 0.88 mmol L^{-1} of methanol, 2.60 mmol L^{-1} of ethanol and 0.049 mmol L^{-1} of acetone. This is a different result than has been observed in the literature, e.g. [22,2,40,50], where methanol was not generated in the same quantities under these conditions; however, ethanol was, like in our results, the primary product. A faradaic efficiency of 96.5% was obtained after 90 min of photoelectrocatalytic reduction, found by considering the number of electrons necessary for methanol, ethanol and acetone formation by the following reactions:

$$CO_2 + 6e^- + 6H^+ \rightleftarrows CH_3OH + H_2O \quad (1)$$

$$CO_2 + 12e^- + 12H^+ \rightleftarrows C_2H_5OH + H_2O \quad (2)$$

$$CO_2 + 16e^- + 16H^+ \rightleftarrows CH_3COCH_3 + H_2O \quad (3)$$

The efficiency of photoelectrocatalytic reduction ($Si/TiO_2/Pt$, UV–vis irradiation and −0.80 V) in relation to photocatalysis ($Si/TiO_2/Pt$ and UV–vis irradiation) and electrolysis ($Si/TiO_2/Pt$ and −0.80 V) was compared by monitoring the CO_2 reduction during 90 min in 0.1 mol L^{-1} $NaHCO_3$ solution, pH 8, saturated with CO_2, by measuring the formation of methanol, ethanol and acetone. Both experiments were able to form only a small amount of acetone as presented in the insert of the Fig. 8b. This comparison confirms CO_2 conversion was more effective under UV–vis irradiation and applied potential.

The mechanism proposed for methanol, ethanol and acetone formation from photoelectrocatalytic CO_2 reduction applied to a p-n junction $Si/TiO_2/Pt$ semiconductor is presented in Fig. 9. The mechanism is proposed in agreement with the literature [22,41,51,52], and is based on e^- and $H^\bullet$ transfer. The possible reaction shows two different pathways; one of them driving to ethanol formation, and the other to acetone. There is probably one preferential pathway in this case, and this fact can explain the dominant formation of ethanol and the small amount of acetone. The methanol could be considered as a sacrificial product that needs to be formed initially for further ethanol or acetone generation.

The $Si/TiO_2/Pt$ semiconductor structure is fundamental for the CO_2 photoelectrocatalytic reduction. The major difficulty in the use of Pt based semiconductor for CO_2 reduction is the possibility to form CO as product. This CO adsorb tightly in the Pt poisoning the electrode [53]. In order to avoid CO formation, the CO_2 needs to be adsorbed in the Pt surface with both oxygen atoms; in that way the carbon is the only one capable to react with other radicals forming oxygenated hydrocarbon products. The use of grid Pt assists the possibility of both oxygen adsorb in the Pt surface, as demonstrated in the mechanism (Fig. 9), due to the distance between Pt nanoparticles, which could be hindered if we had used nanospheres for example.

4. Conclusion

A new and efficient p-n junction $Si/TiO_2/Pt$ semiconductor was constructed based on the heterojunction benefits using lift off and photolithography techniques. The material obtained presents high porosity of both TiO_2 and Pt deposits, in addition to high light absorption in ultraviolet and visible region. Photocurrent vs potential curves showed a characteristic behavior of a p-n junction semiconductor with a good response in the presence of light and CO_2, proving that the CO_2 is a more preferential electron scavenger than water. A small $Si/TiO_2/Pt$ electrode (1 cm^2) was applied in the CO_2 photoelectrocatalytic reduction, confirming the novel electrode is a promising material for photoelectrochemical reduction purposes. The obtained results showed good performance for methanol (0.88 mmol L^{-1}), ethanol (2.60 mmol L^{-1}) and acetone (0.049 mmol L^{-1}) formation as products, presenting 96% of faradaic efficiency. These results were obtained under the best experimental conditions: 0.1 mol L^{-1} $NaHCO_3$, pH 8, saturated with CO_2, 125 W UV–vis light and −0.8 V. Mechanisms of charge transfer at the electrode surface and for products formation have been proposed in order to clarify how the reactions occur.

Acknowledgment

The authors would like to acknowledge Dra. Angela Regina Araújo e Carolina Rabal Biasetto for helpful discussions, and Fapesp (2012/11141-1) and (2013/25343-8) for financial support.

References

[1] F. S. Qin, Y. Xin, X. Liu, W. Ma Yin, Photocatalytic reduction of CO2 in methanol to methyl formate over CuO-TiO2 composite catalysts, J. Colloid Interface Sci. 356 (2011) 257–261, doi:http://dx.doi.org/10.1016/j.jcis.2010.12.034.
[2] J. P. Li, H. Zhang, H. Wang, J. Jing, X. Sui Xu, et al., The photoelectric catalytic reduction of CO2 to methanol on CdSeTe NSs/TiO2 NTs, Catal. Sci. Technol. 4 (2014) 1070, doi:http://dx.doi.org/10.1039/c3cy00978e.
[3] M. Anpo, Photocatalytic reduction of CO2with H2O on highly dispersed Ti-oxide catalysts as a model of artificial photosynthesis, J. CO2 Util. 1 (2013) 8–17, doi:http://dx.doi.org/10.1016/j.jcou.2013.03.005.
[4] S. Hangx, Behaviour of the CO2-H2O system and preliminary mineralisation model and experiments, CATO Work. WP. 1 (2005) 1–43. http://scholar.google.com/scholar?hl=en&btnG=Search&q=intitle:Behaviour+of+the+CO2-H2O+system+and+preliminary+mineralisation+model+and+experiments#0.
[5] M. Halmann, Photoelectrochemical reduction of aqueous carbon dioxide on p-type gallium phosphide in liquid junction solar cells, Nature 275 (1978) 15–16.
[6] B. Aurian-Blajeni, I. Taniguchi, J.O. Bockris, Photoelectrochemical reduction of carbon dioxide using polyaniline-coated silicon, J. Electroanal. Chem. 149 (1983) 291–293.
[7] B.R. Eggins, J.T.S. Irvine, E.P. Murphy, J. Grimshaw, FORMATION OF 2-CARBON ACIDS FROM CARBON-DIOXIDE BY PHOTOREDUCTION ON CADMIUM-SULFIDE, J. Chem. Soc. Chem. Commun. 16 (1988) 1988.
[8] T. Inoue, A. Fujishima, S. Konishi, K. Honda, Photoelectrocatalytic reduction of carbon dioxide in aqueous suspensions of semiconductor powders, Nature 277 (1979) 637–638.
[9] J.F. Brito, A.A. Silva, A.J. Cavalheiro, M.V.B. Zanoni, Evaluation of the Parameters Affecting the Photoelectrocatalytic Reduction of CO 2 to CH 3 OH at Cu / Cu 2 O Electrode, Int. J. Electrochem. Sci. 9 (2014) 5961–5973.
[10] J.F. Brito, A.R. Araujo, K. Rajeshwar, M.V.B. Zanoni, Photoelectrochemical reduction of CO 2 on Cu / Cu 2 O films: Product distribution and pH effects, Chem. Eng. J. 264 (2015) 302–309, doi:http://dx.doi.org/10.1016/j.cej.2014.11.081.
[11] S. Ohya, S. Kaneco, H. Katsumata, T. Suzuki, K. Ohta, Electrochemical reduction of CO2 in methanol with aid of CuO and Cu2O, Catal. Today 148 (2009) 329–334, doi:http://dx.doi.org/10.1016/j.cattod.2009.07.077.

[12] C.W. Li, M.W. Kanan, CO2 reduction at low overpotential on Cu electrodes resulting from the reduction of thick Cu2O films, J. Am. Chem. Soc. 134 (2012) 7231–7234, doi:http://dx.doi.org/10.1021/ja3010978.
[13] Y. Terunuma, Y.M. Saitoh, Relationship between hydrocarbon production in the electrochemical reduction of CO2 and the characteristics of the Cu electrode, J. Electroanal. Chem. 434 (1997) 69–75, doi:http://dx.doi.org/10.1016/s0022-0728(97) 00122-8.
[14] Y. Momose, K. Sato, O. Ohno, Electrochemical reduction of CO2 at copper electrodes and its relationship to the metal surface characteristics, Surf. Interface Anal. 34 (2002) 615–618, doi:http://dx.doi.org/10.1002/sia.1372.
[15] K.P. Kuhl, E.R. Cave, D.N. Abram, T.F. Jaramillo, New insights into the electrochemical reduction of carbon dioxide on metallic copper surfaces, Energy Environ. Sci. 5 (2012) 7050, doi:http://dx.doi.org/10.1039/c2ee21234j.
[16] K. Rajeshwar, N.R. De Tacconi, G. Ghadimkhani, W. Chanmanee, C. Janáky, Tailoring copper oxide semiconductor nanorod arrays for photoelectrochemical reduction of carbon dioxide to methanol, ChemPhysChem 14 (2013) 2251–2259, doi:http://dx.doi.org/10.1002/cphc.201300080.
[17] W. Siripala, A. Ivanovskaya, T.F. Jaramillo, S.H. Baeck, E.W. McFarland, A Cu2O/TiO2 heterojunction thin film cathode for photoelectrocatalysis, Sol. Energy Mater. Sol. Cells 77 (2003) 229–237, doi:http://dx.doi.org/10.1016/s0927-0248(02) 00343-4.
[18] P.E. de Jongh, D. Vanmaekelbergh, J.J. Kelly, Photoelectrochemistry of Electrodeposited Cu2O, J. Electrochem. Soc. 147 (2000) 486, doi:http://dx.doi.org/10.1149/1.1393221.
[19] A. Paracchino, V. Laporte, K. Sivula, M. Grätzel, E. Thimsen, Highly active oxide photocathode for photoelectrochemical water reduction, Nat. Mater. 10 (2011) 456–461, doi:http://dx.doi.org/10.1038/nmat3017.
[20] Z. Zhang, P. Wang, Highly stable copper oxide composite as an effective photocathode for water splitting via a facile electrochemical synthesis strategy, J. Mater. Chem. 22 (2012) 2456, doi:http://dx.doi.org/10.1039/c1jm14478b.
[21] J. Cheng, M. Zhang, G. Wu, X. Wang, J. Zhou, K. Cen, Photoelectrocatalytic Reduction of CO 2 into Chemicals Using Pt- Modi fi ed Reduced Graphene Oxide Combined with Pt-Modi fi ed TiO 2 Nanotubes, Environ. Sci. Technol. 48 (2014) 7076–7084.
[22] J. Z. Yang, C. Xu, H. Wu, P. Jing, H. Yin Li, New insight into photoelectric converting CO2 to CH3OH on the one-dimensional ribbon CoPc enhanced Fe2O3 NTs, Appl. Catal. B Environ. 156-157 (2014) 249–256, doi:http://dx.doi.org/10.1016/j.apcatb.2014.03.012.
[23] Y.J. Hwang, A. Boukai, P. Yang, High Density n-Si / n-TiO 2Core / Shell Nanowire Arrays with Enhanced Photoactivity 2009, Nano Lett. 9 (2009) 410–415, doi:http://dx.doi.org/10.1021/nl8032763.
[24] K. S.Y. Noh, C. Sun, M. Choi, M. Niu, K. Xu Yang, et al., Branched TiO2/Si nanostructures for enhanced photoelectrochemical water splitting, Nano Energy 2 (2013) 351–360, doi:http://dx.doi.org/10.1016/j.nanoen.2012.10.010.
[25] R. Kontic, G.R. Patzke, Synthetic trends for BiVO 4 photocatalysts: Molybdenum substitution vs. TiO 2 and SnO 2 heterojunctions, J. Solid State Chem. 189 (2012) 38–48, doi:http://dx.doi.org/10.1016/j.jssc.2011.11.050.
[26] M.J. Madou, Fundamentals of microfabrication and nanotechnology, 3rd ed., CRC, Boca Raton: CRC, 2012, pp. 670.
[27] H. Yu, S. Chen, X. Quan, H. Zhao, Y. Zhang, Silicon nanowire/TiO2 heterojunction arrays for effective photoelectrocatalysis under simulated solar light irradiation, Appl. Catal. B Environ. 90 (2009) 242–248, doi:http://dx.doi.org/10.1016/j.apcatb.2009.03.010.
[28] P.A. Christensen, M.A. Carroll, D. Linares-Moya, D. Molyneux, M.C. Rosamond, D. Wood, A Novel Composite Anode: The Electrooxidation of Organic Molecules via Formation of Highly Energetic Holes, J. Phys. Chem. C 115 (2011) 10777–10783, doi:http://dx.doi.org/10.1021/jp202325m.
[29] P.A. Christensen, T.A. Egerton, W.F. Lin, P. Meynet, Z.-G. Shao, N.G. Wright, A novel electrochemical device for the disinfection of fluids by OH radicals, Chem. Commun. (Camb.) (2006) 4022–4023, doi:http://dx.doi.org/10.1039/b608329n.
[30] G. Liu, N. Hoivik, K. Wang, H. Jakobsen, Engineering TiO 2 nanomaterials for CO 2 conversion/solar fuels, Sol. Energy Mater. Sol. Cells 105 (2012) 53–68, doi:http://dx.doi.org/10.1016/j.solmat.2012.05.037.
[31] M.F. Brugnera, K. Rajeshwar, J.C. Cardoso, M.V.B. Zanoni, Bisphenol A removal from wastewater using self-organized TIO(2) nanotubular array electrodes, Chemosphere 78 (2010) 569–575, doi:http://dx.doi.org/10.1016/j.chemosphere.2009.10.058.
[32] J. Tauc, R. Grigorovici, A. Vancu, Optical Properties and Electronic Structure of Amorphous Germanium, Phys. Status Solidi 15 (1966) 627–637.
[33] G.G. Bessegato, J.C. Cardoso, M.V.B. Zanoni, Enhanced photoelectrocatalytic degradation of an acid dye with boron-doped TiO2 nanotube anodes, Catal. Today (2015) , doi:http://dx.doi.org/10.1016/j.cattod.2014.03.073.
[34] G.G. Bessegato, J.C. Cardoso, M.V.B. Zanoni, Enhanced photoelectrocatalytic degradation of an acid dye with boron-doped TiO2 nanotube anodes, Catal. Today (2014) , doi:http://dx.doi.org/10.1016/j.cattod.2014.03.073.
[35] R. López, R. Gómez, Band-gap energy estimation from diffuse reflectance measurements on sol-gel and commercial TiO 2: A comparative study, J. Sol-Gel Sci. Technol. 61 (2012) 1–7, doi:http://dx.doi.org/10.1007/s10971-011-2582-9.
[36] T.T. Guaraldo, T.B. Zanoni, S.I.C. de Torresi, V.R. Gonçales, G.J. Zocolo, D.P. Oliveira, et al., On the application of nanostructured electrodes prepared by Ti/TiO2/WO3 template: a case study of removing toxicity of indigo using visible irradiation, Chemosphere 91 (2013) 586–593, doi:http://dx.doi.org/10.1016/j.chemosphere.2012.12.027.
[37] L. Jing, B. Xin, F. Yuan, L. Xue, B. Wang, H. Fu, Effects of surface oxygen vacancies on photophysical and photochemical processes of Zn-doped TiO2 nanoparticles and their relationships, J. Phys. Chem. B 110 (2006) 17860–17865, doi:http://dx.doi.org/10.1021/jp063148z.
[38] Y. Cai, Y. Ye, Z. Tian, J. Liu, Y. Liu, C. Liang, In situ growth of lamellar ZnTiO3 nanosheets on TiO2 tubular array with enhanced photocatalytic activity, Phys. Chem. Chem. Phys. 15 (2013) 20203–20209, doi:http://dx.doi.org/10.1039/c3cp53307g.
[39] H. Wang, J.L. Faria, S. Dong, Y. Chang, Mesoporous Au/TiO2 composites preparation, characterization, and photocatalytic properties, Mater. Sci. Eng. B 177 (2012) 913–919, doi:http://dx.doi.org/10.1016/j.mseb.2012.04.015.
[40] G. Ghadimkhani, N.R. De Tacconi, W. Chanmanee, C. Janaky, K. Rajeshwar, Chemical Communications, Chem. Commun. 49 (2013) 1297–1299, doi:http://dx.doi.org/10.1039/c2cc38068d.
[41] M. Tahir, N.S. Amin, Advances in visible light responsive titanium oxide-based photocatalysts for CO2 conversion to hydrocarbon fuels, Energy Convers. Manag. 76 (2013) 194–214.
[42] T.T. Guaraldo, S.H. Pulcinelli, M.V.B. Zanoni, Influence of particle size on the photoactivity of Ti/TiO2 thin film electrodes, and enhanced photoelectrocatalytic degradation of indigo carmine dye, J. Photochem. Photobiol. A Chem. 217 (2011) 259–266, doi:http://dx.doi.org/10.1016/j.jphotochem.2010.10.019.
[43] C. Wang, X. Ma, J. Li, L. Xu, F. Zhang, Reduction of CO 2 aqueous solution by using photosensitized-TiO 2 nanotube catalysts modified by supramolecular metalloporphyrins-ruthenium (II) polypyridyl complexes, J. Mol. Catal. A Chem. 364 (2012) 108–114.
[44] S. Ikeda, T. Takagi, K. Ito, Selective Formation of Formic Acid, Oxalic Acid, and Carbon Monoxide by Electrochemical Reduction of Carbon Dioxide, Bull. Chem. Soc. Jpn. 60 (1987) 2517–2522.
[45] N.M. Dimitrijevic, B.K. Vijayan, O.G. Poluektov, T. Rajh, K. a Gray, H. He, et al., Role of water and carbonates in photocatalytic transformation of CO2 to CH4 on titania, J. Am. Chem. Soc. 133 (2011) 3964–3971, doi:http://dx.doi.org/10.1021/ja108791u.
[46] M.M. Halmann, M. Steinberg, Greenhouse gas carbon dioxide mitigation: science and technology, 6th ed., Fla: Lewis Publishers, Boca Raton, 1999.
[47] L.J. Minggu, K.H. Ng, H.A. Kadir, M. Bin Kassim, Bilayer n-WO3/p-Cu2O photoelectrode with photocurrent enhancement in aqueous electrolyte photoelectrochemical reaction, Ceram. Int. 40 (2014) 16015–16021, doi:http://dx.doi.org/10.1016/j.ceramint.2014.07.135.
[48] J.N. Butler, Carbon dioxide equilibria and their applications, Addison-Wesley, 1982.
[49] R.E. Zeebe, D. Wolf-Gladrow, CO2 in seawater: Equilibrium kinetics, isotopes, Elsevier Oceanogr. Ser. 65 (2001) 1–346.
[50] P. Li, J. Xu, H. Jing, C. Wu, H. Peng, J. Lu, et al., Wedged N-doped CuO with more negative conductive band and lower overpotential for high efficiency photoelectric converting CO2 to methanol, Appl. Catal. B Environ. 156–157 (2014) 134–140, doi:http://dx.doi.org/10.1016/j.apcatb.2014.03.011.
[51] M. Gattrell, N. Gupta, A. Co, A review of the aqueous electrochemical reduction of CO2 to hydrocarbons at copper, J. Electronal. Chem. 594 (2006) 1–19, doi:http://dx.doi.org/10.1016/j.jelechem.2006.05.013.
[52] G.K. Ramesha, J.F. Brennecke, P.V. Kamat, The Origin of Catalytic Effect in the Reduction of CO2 at Nanostructured TiO2 Films, ACS Catal. 4 (2014) 3249–3254, doi:http://dx.doi.org/10.1021/cs500730w.
[53] X.-G. Zhang, P.B. Armentrout, Activation of O 2, CO, and CO 2 by Pt +: The Thermochemistry of PtO +, J. Phys. Chem. A 107 (2003) 8904–8914, doi:http://dx.doi.org/10.1021/jp036014j.